Int. J. Heat Mass Transfer. Vol. 25, No. 6, pp. 863–870, 1982.
Printed in Great Britain

0017-9310/82/060863-08 $03.00/0

ELLIPTIC FIELD CALCULATION OF A LAMINAR DIFFUSION FLAME ADJACENT TO A VERTICAL FLAT PLATE BURNER

V. K. LIU*, K. T. YANG and J. R. LLOYD

Department of Aerospace and Mechanical Engineering, University of Notre Dame, Notre Dame, IN 46556, U.S.A.

(*Received* 15 *December* 1981)

Abstract—This numerical study deals with the phenomenon of a diffusion flame on a vertical plate burner with methane injection. The unsteady governing conservation equations along with an exponential wide-band model for gas radiation and an infinite reaction rate model for combustion are solved by finite-difference calculations. The numerical results are then compared with those of both the local non-similarity boundary-layer solution and the experimental data obtained in a previous study. It is shown that the finite-difference calculations produce results in better agreement with the experimental data in the region outside the flame sheet.

NOMENCLATURE

C, $U_R^2/(R_R T_R)$;
c_p, mixture specific heat [J K^{-1} g^{-1}];
D, mass diffusion coefficient [cm^2 s^{-1}];
F, gH/U_R^2;
g, gravitational acceleration [cm s^{-2}];
H, reference length [cm];
h, enthalpy of gas mixture [J g^{-1}];
I, J, cell indices;
$\mathbf{J}$, diffusive mass flux [g s^{-1} cm^{-2}];
k, mixture thermal conductivity [J s^{-1} cm^{-1} K^{-1}];
M, molecular weight [g mol^{-1}];
$\dot{M}'''$, volumetric mass generation rate [g s^{-1} cm^{-3}];
N_R, $\sigma T_R^4/(\rho_R c_{pR} U_R T_R)$;
Pr, Prandtl number;
p, pressure [atm.];
Q, heat of combustion [J g^{-1} mol^{-1}];
$\dot{Q}'''$, volumetric heat generation rate [J s^{-1} cm^{-3}];
Q_{CT}, $Q/(c_{pR} T_R)$;
$\mathbf{q}_c''$, conductive heat flux [J s^{-1} cm^{-2}];
$\mathbf{q}_R''$, total radiative flux [J s^{-1} cm^{-2}];
R, gas constant [J g^{-1} K^{-1}];
Sc, Schmidt number;
T, absolute temperature [K];
t, time [s];
U_R, reference velocity [cm s^{-1}];
u, v, velocity components of gas mixture in the x, y directions, respectively [cm s^{-1}];
W, $(\hat{Y} - \hat{Y}_O + \hat{Y}_{O,R})Q_{CT}$;
x, coordinate normal to plate [cm];
x_R, location of x at edge of computation domain [cm];
Y, mass concentration;
$\hat{Y}$, $Y/[M(v'' - v')]$;
y, coordinate along the plate [cm].

Greek symbols

Δt, time step [s];
Δx, cell step size in x-direction [cm];
Δy, cell step size in y-direction [cm];
θ, $\hat{h} - (\hat{Y}_O - \hat{Y}_{O,R})Q_{CT}$
μ, mixture dynamic viscosity [g s^{-1} cm^{-1}]
v', stoichiometric coefficient of reactant;
v'', stoichiometric coefficient of product;
ρ, mixture density [g cm^{-3}];
σ, Stefan–Boltzmann constant [J s^{-1} cm^2 K^{-4}];
τ, stress tensor [g cm^{-2}].

Subscripts

C, CO_2;
E, equilibrium condition;
F, fuel;
H, H_2O;
N, N_2;
O, O_2;
P, product of combustion;
R, reference conditions;
w, wall conditions;
x, x-components;
y, y-components;
α, species.

Superscripts

α, species;
$\sim$, dimensionless quantities.

* Present address: Shell Development Company, Houston, Texas, U.S.A.

INTRODUCTION

IN A RECENT study [1] on a diffusion flame adjacent to a vertical flat plate burner, the flow, temperature and species concentration fields, including the effects of 1-dim. surface and gaseous radiation, were calculated on the basis of a local non-similarity solution to the governing equations and compared with experimental data obtained with a Mach–Zehnder interferometer. The analytical results show satisfactory agreement with the observed data in terms of the temperature variations within the flame, the peak temperature resulting from the combustion process, and the fuel surface heat transfer, but underestimate the overall boundary-layer thickness. It has been postulated that this latter discrepancy is primarily a result of the development of the thermal boundary-layer formed below the porous burner plate leading edge in the experimental situation. While the validity of this postulate is not beyond question, the upstream thermal boundary-layer does exist nevertheless, as can be clearly seen in a typical interferogram shown in Fig. 1. In order to more adequately describe the far fields away from the flame sheet and the interaction of the flame layer with the thermal field below the porous burner, the boundary-layer assumptions and the local non-similarity solution which possesses a singularity at the burner leading edge must be discarded in favor of the set of complete governing differential equations and their solutions for the same diffusion flame problem. In the present study, such a solution based on finite-difference calculations of the governing elliptic field equations has been obtained. The effects of variable properties and 1-dim. surface and gaseous radiation are also retained in view of their significance in the diffusion flame problem [1].

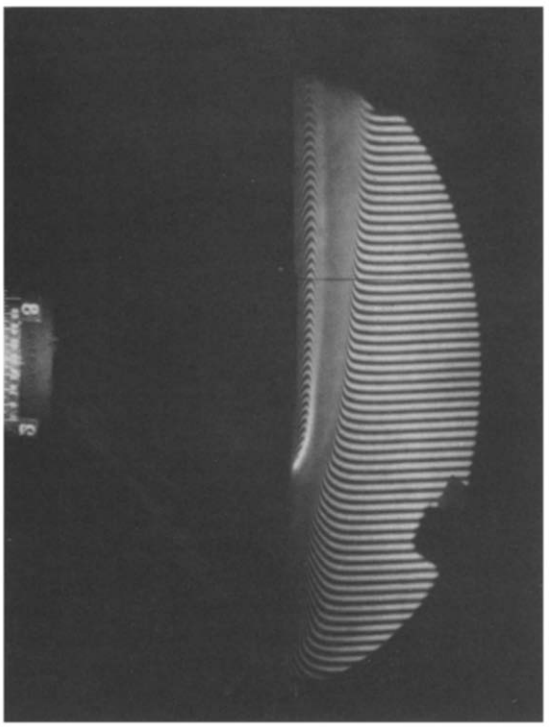

FIG. 1. Interferogram of methane diffusion flame.

Another important objective of the elliptic field calculations here is to demonstrate the methodology of such calculations as applied to predominantly boundary-layer type of phenomena. There are many such phenomena in nature as well as in practical applications where the boundary-layer assumptions are only valid in certain regions of the flow and consequently the corresponding boundary-layer solutions do not adequately describe the overall fields that are of interest. The elliptic field calculations as utilized in the present study will help to fill this gap in the solution methodologies that are currently available to us.

Finally, it should also be pointed out that while elliptic-field, finite-difference calculations are not new, the present solution is by no means trivial in view of the inclusion of species concentration, variable properties and non-gray gaseous radiation.

THE GOVERNING EQUATIONS

The problem under consideration here deals with a steady laminar diffusion flame adjacent to a vertical porous plate, through which methane is injected. More details of the physical situation are given in [1]. The coordinate system utilized in this study is shown in Fig. 2. It is seen that the calculation field is divided into three separate regions. Region I lies below the burner leading edge, Region II includes the boundary-layer region next to the porous plate, and Region III is above the trailing edge of the burner. The governing equations for the entire field of calculations are given as follows:

Perfect-gas law for the gas mixture

$$p = \rho RT \tag{1}$$

Conservation equation for the total mass

$$\frac{\partial \rho}{\partial t} + \frac{\partial}{\partial x}(\rho u) + \frac{\partial}{\partial y}(\rho v) = 0 \tag{2}$$

Chemical reaction equation for burning methane

$$\nu'_F(CH_4) + \nu'_O(O_2) + \nu'_O(3.74\,N_2) + \nu'_H(H_2O) + \nu'_C(CO_2) \rightarrow \nu''_F(CH_4) + \nu''_O(O_2) + \nu''_O(3.74N_2) + \nu''_H(H_2O) + \nu''_C(CO_2) + Q \tag{3}$$

where Q is the heat of combustion [2] and the stoichiometric constants are

$$\nu'_F = 1,\ \nu'_O = 2,\ \nu'_H = 0,\ \nu'_C = 0,\ \nu''_F = 0,$$
$$\nu''_O = 0,\ \nu''_H = 2,\ \text{and}\ \nu''_C = 1.$$

It is noted here that the reaction rate is taken to be

infinite and that there are five gas species: CH_4, O_2, N_2, CO_2, and H_2O.

Conservation equations for individual gas species

$$\frac{\partial}{\partial t}(\rho Y_\alpha) + \frac{\partial}{\partial x}(\rho u Y_\alpha) + \frac{\partial}{\partial y}(\rho v Y_\alpha) = -\frac{\partial J_x^\alpha}{\partial x} - \frac{\partial J_y^\alpha}{\partial y} + \dot{M}_\alpha''' \quad (4)$$

where α refers to a gas species. For convenience, only three of these equations will be utilized for methane, oxygen and the combined combustion products of H_2O and CO_2. The mass concentration for N_2 is simply given by

$$Y_N = 1 - Y_F - Y_O - Y_P \quad (5)$$

and Y_P is defined by

$$Y_P = Y_H + Y_O.$$

Conservation equations for momentum

$$\frac{\partial}{\partial t}(\rho u) + \frac{\partial}{\partial x}(\rho u^2) + \frac{\partial}{\partial y}(\rho u v) = -\frac{\partial(p - p_E)}{\partial x} + \frac{\partial \tau_{xx}}{\partial x} + \frac{\partial \tau_{xy}}{\partial y} \quad (6)$$

$$\frac{\partial}{\partial t}(\rho v) + \frac{\partial}{\partial x}(\rho u v) + \frac{\partial}{\partial y}(\rho v^2) = -\frac{\partial(p - p_E)}{\partial y} - (\rho - \rho_E)g + \frac{\partial \tau_{yx}}{\partial x} + \frac{\partial \tau_{yy}}{\partial y} \quad (7)$$

where the subscript E refers to hydrostatic equilibrium conditions.

Conservation equation for energy

$$\frac{\partial}{\partial t}(\rho h) + \frac{\partial}{\partial x}(\rho u h) + \frac{\partial}{\partial y}(\rho v h) = -\frac{\partial q_x}{\partial x} - \frac{\partial q_y}{\partial y} - \frac{dq_R''}{dx} + Q''' \quad (8)$$

where h is the enthalpy of the gas mixture defined by

$$h = \int_{T_R}^{T} c_p \, dT \qquad c_p = \sum_\alpha Y_\alpha c_p^\alpha \quad (9)$$

and the radiation flux q_R'' is taken to be 1-dim. Also it is noted that in equation (8) viscous dissipation and pressure work are both neglected.

The mass, momentum and heat fluxes in the above equations can be described as

$$J_x^\alpha = -D\frac{\partial Y_\alpha}{\partial x} \qquad J_y^\alpha = -D\frac{\partial Y_\alpha}{\partial y} \quad (10)$$

$$\tau_{xx} = 2\mu\frac{\partial u}{\partial x} \qquad \tau_{xy} = \tau_{yx} = \mu\left(\frac{\partial u}{\partial y} + \frac{\partial v}{\partial x}\right) \qquad \tau_{yy} = 2\mu\left(\frac{\partial v}{\partial y}\right) \quad (11)$$

$$q_x = -k\frac{\partial T}{\partial x} \qquad q_y = -k\frac{\partial T}{\partial y} \quad (12)$$

respectively, and μ and k are respectively the mixture dynamic viscosity and thermal conductivity evaluated in accordance with [3–5].

It is noted here that all governing conservation equations are for unsteady flows for expediency in the numerical calculations, even though only steady results are sought. As a result, initial conditions are needed to initiate the computations. In the present study, results from the local similarity solution [1] are used for Region II (Fig. 2). In Region I, the initial conditions are given by the values at the lowest row in Region II, and similarly for Region III, values at the highest row in Region II are taken to be the initial conditions. Also, velocity components v are arbitrarily doubled with respect to their original values from the analytical results to enhance the convergence process.

The extent of the physical computation domain in the x-direction, x_R, is chosen such that variables at this boundary (Fig. 2) can be considered to be those corresponding to the undisturbed condition. In this study, x_R is set approx. 20 times the thickness of the flame region, which varies between 2 and 4 mm. At $x = x_R$ (all Regions)

$$\left.\begin{aligned} &T = T_R, \\ &Y_H = Y_C = Y_F = 0, \quad Y_O = 0.232, \\ &\qquad\qquad Y_N = 0.768, \\ &\frac{\partial u}{\partial x} = \frac{\partial v}{\partial x} = 0, \qquad p = 1 \text{ atm}. \end{aligned}\right\} \quad (13)$$

The gas velocity gradients or the natural boundary conditions are utilized here as sufficient conditions for the undisturbed region. In Region I, the pure boundary-layer flow develops along the insulated plate without fuel injection and chemical reaction. The temperatures on the wall can be set either at the ambient condition or with the measured values. On the wall for this region at $x = 0$, we have

$$\left.\begin{aligned} &T = T_R \quad \text{or} \quad T = T_w(y), \\ &u = v = 0, \quad Y_F = Y_H = Y_C = 0, \\ &\frac{\partial Y_O}{\partial x} = \frac{\partial Y_N}{\partial x} = 0, \quad p = 1 \text{ atm}. \end{aligned}\right\} \quad (14)$$

Boundary conditions at $x = 0$ for Region II may be written as

$$\left.\begin{aligned} &T = T_w(y) \quad \text{(measured)}, \\ &u = u_w \text{ (constant)}, \quad v = 0, \\ &u_w(1 - Y_F) = -D\left(\frac{\partial Y_F}{\partial x}\right), \\ &u_w(1 - Y_P) = -D\left(\frac{\partial Y_P}{\partial x}\right), \\ &Y_O = 0, \ \frac{\partial Y_N}{\partial x} = 0, \quad p = 1 \text{ atm}. \end{aligned}\right\} \quad (15)$$

In Region III no fuel injection occurs at the insulated wall, but the combustion process still continues. The surface temperatures can either be the measured values or calculated from the condition that the sum of radiative and conduction fluxes is zero. The corresponding conditions at $x = 0$ are

$$\left.\begin{aligned} &T = T_w(y) \quad \text{or} \quad \dot{q}''_R + \dot{q}''_C = 0 \\ &u = v = 0, \\ &\frac{\partial Y_F}{\partial x} = \frac{\partial Y_O}{\partial x} = \frac{\partial Y_P}{\partial x} = 0, \quad p = 1\ \text{atm.} \end{aligned}\right\} \quad (16)$$

At the lower boundary of Region I, $y = 0$, the boundary conditions are

$$\left.\begin{aligned} &T = T_R \quad \text{or} \quad T = T_0(x) \quad \text{(measured)}, \\ &\frac{\partial u}{\partial y} = \frac{\partial v}{\partial y} = 0, \\ &Y_F = Y_P = 0, \quad Y_O = 0.232, \quad Y_N = 0.768, \\ &\qquad\qquad p = 1\ \text{atm.} \end{aligned}\right\} \quad (17)$$

Note that the natural boundary conditions for the flow are again utilized here. At the top of Region III, the boundary conditions there are

$$\left.\begin{aligned} &\frac{\partial T}{\partial y} = 0 \quad \text{for } v > 0 \quad \text{or} \quad T = T_R \quad \text{for } v \leqslant 0, \\ &\frac{\partial u}{\partial y} = \frac{\partial v}{\partial y} = 0, \quad \frac{\partial Y_F}{\partial y} = \frac{\partial Y_O}{\partial y} = \frac{\partial Y_P}{\partial y} = 0, \\ &p = 1\ \text{atm.} \end{aligned}\right\} \quad (18)$$

Among the five gas species in the diffusion plane, only H_2O, CO_2 and CH_4 absorb and emit thermal energy. The contribution to the total radiative flux from each gas band under non-homogeneous conditions is evaluated in the present study on the basis of the exponential wide-band model [6, 7] and the scaling approximation for radiation parameters [8, 9]. However, only 1-dim. gas radiation flux is considered. Detailed formulation for the radiation flux term in the energy equation (8) covering both individual and overlapping bands is given in [1, 10], and hence will not be repeated here. As mentioned previously, the reaction rates in the methane diffusion flame are taken to be infinite, and therefore the thickness of the flame sheet becomes infinitesimal, and stoichiometric conditions prevail. In addition, the species mass production rate $\dot{M}'''_\alpha$ in equation (4) and the heat generation quantity $\dot{Q}'''$ in equation (8) are related to each other as follows:

$$\frac{\dot{M}'''_F}{M_F(v''_F - v'_F)} = \frac{\dot{M}'''_O}{M_O(v''_O - v'_O)} = \frac{\dot{M}'''_P}{M_P(v''_P - v'_P)} = \frac{\dot{Q}'''}{Q} \quad (19)$$

where M_α is the molecular weight of species α.

For convenience, the governing differential equations may now be cast into dimensionless forms, as given in the following [10]:

$$C\tilde{p} = \tilde{\rho}\tilde{R}\tilde{T} - e^{-(C/F)\tilde{v}}, \quad (20)$$

$$\frac{\partial\tilde{\rho}}{\partial\tilde{t}} + \frac{\partial}{\partial\tilde{x}}(\tilde{\rho}\tilde{u}) + \frac{\partial}{\partial\tilde{y}}(\tilde{\rho}\tilde{v}) = 0, \quad (21)$$

$$\frac{\partial}{\partial\tilde{t}}(\tilde{\rho}W_F) + \frac{\partial}{\partial\tilde{x}}(\tilde{\rho}\tilde{u}W_F) + \frac{\partial}{\partial\tilde{y}}(\tilde{\rho}\tilde{v}W_F) = \frac{\partial}{\partial\tilde{x}}\left[\left(\frac{\tilde{\mu}}{Sc}\right)\frac{\partial W_F}{\partial\tilde{x}}\right] + \frac{\partial}{\partial\tilde{y}}\left[\left(\frac{\tilde{\mu}}{Sc}\right)\frac{\partial W_F}{\partial\tilde{y}}\right], \quad (22)$$

$$\frac{\partial}{\partial\tilde{t}}(\tilde{\rho}W_P) + \frac{\partial}{\partial\tilde{x}}(\tilde{\rho}\tilde{u}W_P) + \frac{\partial}{\partial\tilde{y}}(\tilde{\rho}\tilde{v}W_P) = \frac{\partial}{\partial\tilde{x}}\left[\left(\frac{\tilde{\mu}}{Sc}\right)\frac{\partial W_P}{\partial\tilde{x}}\right] + \frac{\partial}{\partial\tilde{y}}\left[\left(\frac{\tilde{\mu}}{Sc}\right)\frac{\partial W_P}{\partial\tilde{y}}\right] \quad (23)$$

$$\frac{\partial}{\partial\tilde{t}}(\tilde{\rho}\tilde{u}) + \frac{\partial}{\partial\tilde{x}}(\tilde{\rho}\tilde{u}^2) + \frac{\partial}{\partial\tilde{y}}(\tilde{\rho}\tilde{u}\tilde{v}) = -\frac{\partial\tilde{p}}{\partial\tilde{x}} + \frac{\partial\tilde{\tau}_{xx}}{\partial\tilde{x}} + \frac{\partial\tilde{\tau}_{xy}}{\partial\tilde{y}}, \quad (24)$$

$$\frac{\partial}{\partial\tilde{t}}(\tilde{\rho}\tilde{v}) + \frac{\partial}{\partial\tilde{x}}(\tilde{\rho}\tilde{u}\tilde{v}) + \frac{\partial}{\partial\tilde{y}}(\tilde{\rho}\tilde{v}^2) = -\frac{\partial\tilde{p}}{\partial\tilde{y}} - \frac{1}{F}(\tilde{\rho} - \tilde{\rho}_E) + \frac{\partial\tilde{\tau}_{yx}}{\partial\tilde{x}} + \frac{\partial\tilde{\tau}_{yy}}{\partial\tilde{y}}, \quad (25)$$

$$\frac{\partial}{\partial\tilde{t}}(\tilde{\rho}\theta) + \frac{\partial}{\partial\tilde{x}}(\tilde{\rho}\tilde{u}\theta) + \frac{\partial}{\partial\tilde{y}}(\tilde{\rho}\tilde{v}\theta) = \frac{\partial}{\partial\tilde{x}}\left[\left(\frac{\tilde{\mu}}{Pr}\right)\frac{\partial\theta}{\partial\tilde{x}}\right] + \frac{\partial}{\partial\tilde{y}}\left[\left(\frac{\tilde{\mu}}{Pr}\right)\frac{\partial\theta}{\partial\tilde{y}}\right] - N_R\frac{d\tilde{q}''_R}{d\tilde{x}}, \quad (26)$$

where

$$\tilde{x} = \frac{x}{H}, \quad \tilde{y} = \frac{y}{H}, \quad \tilde{t} = \frac{u}{U_R}$$

$$\tilde{u} = \frac{u}{U_R}, \quad \tilde{v} = \frac{v}{U_R}, \quad \tilde{T} = \frac{T}{T_R}, \quad \tilde{\rho} = \frac{\rho}{\rho_R},$$

$$\tilde{p} = \frac{p - p_E}{\rho_R U_R^2}, \quad \tilde{p}_E = \frac{p_E}{\rho_R R_R T_R},$$

$$c_P = \sum_\alpha Y_\alpha c''_P, \quad \tilde{c}_P = \frac{1}{T - T_R}\int_{T_R}^{T} c_P dT, \quad \tilde{\bar{c}} = \frac{\tilde{c}_P}{c_{PR}},$$

$$\tilde{c}_P = \frac{c_P}{c_{PR}}, \quad \tilde{R} = \frac{R}{R_R} = \sum_\alpha \frac{Y_\alpha}{\tilde{M}_\alpha}, \quad \tilde{M}_\alpha = \frac{M_\alpha}{M_R},$$

$$W_\alpha = (\hat{Y}_\alpha - \hat{Y}_O + \hat{Y}_{O,R})Q_{CT}$$

$$\theta = \tilde{h} - (\hat{Y}_O - \hat{Y}_{O,R})Q_{C,T}$$

$$\hat{Y}_\alpha = \frac{Y_\alpha}{M_\alpha(v''_\alpha - v'_\alpha)}, \quad \tilde{h} = \frac{h}{c_{PR}T_R}, \quad Q_{CT} = \frac{Q}{c_{PR}T_R},$$

$$Pr = \frac{\mu c_P}{k}, \quad Sc = \frac{\nu}{D}, \quad \tilde{\mu} = \frac{\mu}{\rho_R U_R H}, \quad \tilde{\tau} = \frac{\tau}{\rho_R U_R^2},$$

$$\tilde{q}''_R = \frac{\dot{q}''_R}{\sigma T_R^4}, \quad N_R = \frac{\sigma T_R^4}{\rho_R U_R c_{PR} T_R}.$$

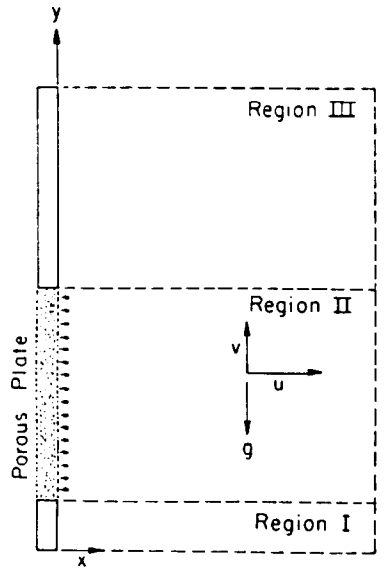

FIG. 2. Coordinate system and computation domain.

The boundary conditions can be similarly treated. The subscript R in the above equations refers to a reference condition, which can be arbitrarily chosen. Furthermore, in view of the presence of the local c_p, the Prandtl number Pr is also taken to be local.

FINITE-DIFFERENCE CALCULATIONS

The formation of the finite-difference equations is based on the control-volume scheme with upwind differencing for the convection terms, the calculation procedure involves the use of staggered cells for the two velocity components and a modified pressure correction scheme is used to satisfy the mass continuity to accommodate the boundary-layer behaviors [10, 11]. There has been much controversy regarding the accuracy of the upwind difference calculations in the recent literature [11]. In the present study, the maximum cell Peclet number is of the order of 10, and the upwind-differencing scheme is expected to be quite adequate. Furthermore, since the velocity vector is essentially all in the positive $\bar{y}$ direction, the effect of artificial diffusion should not be serious. Fig. 3 shows the cell dimensions in the computational domain; together with the overall physical dimensions corresponding to the experimental configurations [1]. The step size Δy is taken to be a constant of 1 mm, and Δx varies from 0.3 mm in the wall region to 2 mm at $I = NI$. More specifically, there are 10 cells from the wall to the flame sheet and Δx is increased uniformly to approx. 3 mm at the flame sheet location. It is further increased by 10% each step until $\Delta x = 2\,\Delta y$, or 2 mm. Thereafter, Δx is kept at 2 mm until I reaches 42. The thickness of the thermal boundary-layer is about 0.9–1.1 cm. The present choice of the cell structure in

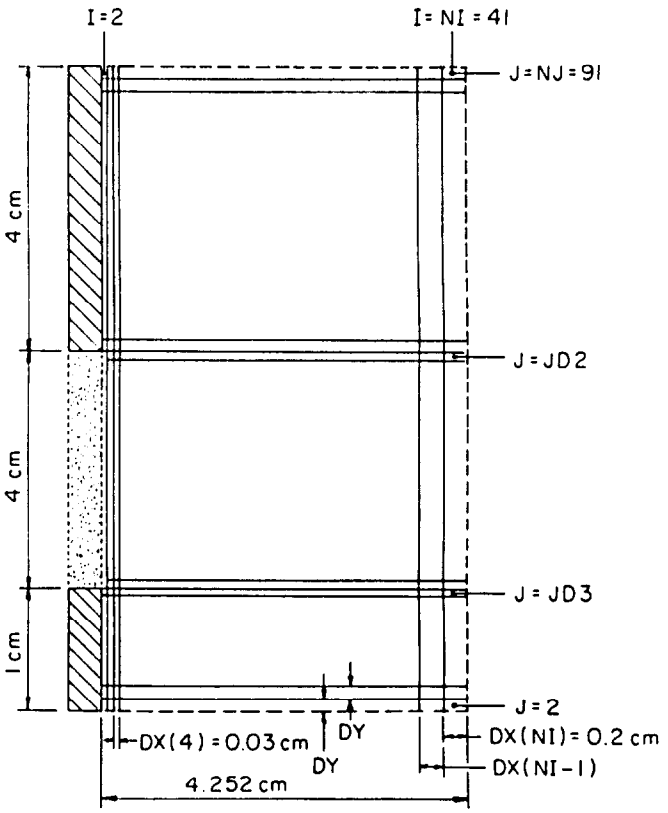

FIG. 3. Cell dimensions in computation domain.

the computation domain leads to a value of x_R about four times that of the thermal boundary-layer, thus insuring the adequacy of the undisturbed conditions at $x = x_R$. A time step of $\Delta t = 0.005$ is utilized throughout the calculations.

All properties including the specific heat of the gas mixture and the radiative heat flux and its derivative are evaluated at the old time step. The sequence of calculations is as follows: the energy equation is first solved, followed by the solutions to the two species equations. Then the density of the mixture is evaluated from the equation of state. From here, the two velocity components and the pressure can be solved from the two momentum equations and the pressure correction equation through an iterative calculation. Details of the flow chart, error control routine, and sweeping schemes for handling the tridiagonal matrices are given in [10].

RESULTS AND DISCUSSION

The burning porous plate used in the experiment [1] was held in position by insulated materials around its edges, and then it was squeezed into an outer frame. With the diffusion flame adjacent to the vertical porous surface, the thermal boundary-layer did not begin to develop from the bottom edge of the burning plate, but rather started its development from the bottom of the frame, as can be seen in Fig. 1. It is interesting to determine the quantitative effect of the preheated air flow upstream of the burning plate, and this can only be done with the elliptic field calculations in the present study. The temperature profile was measured along $y = 0$, and has been used as the horizontal free boundary condition for Region I. The following observation can be made from the numerical results for the case of a methane flow rate of 1.40 l min^{-1}, and an injection speed of 0.6 cm s^{-1}: Before the flow reaches the porous plate, the air boundary-layer is already 6 mm thick. In the combustion Region II at the vertical position of $y = 1.05$ cm; the temperature at $x = 0.369$ cm is 30 K above the temperature according to the boundary-layer calculations, and the thermal boundary thickness is already 6.5 mm as compared to 3.7 mm for the boundary-layer solution case. This augmentation of the thermal boundary-layer thickness then decreases until $y = 3.25$ cm, beyond which the effect of the preheated air layer at $y = 0$ becomes insignificant. At this point and beyond, the heat transfer process is completely dominated by the high flame temperature and the effect of mass diffusion resulting from the combustion process.

For the same experimental case, temperature profiles from the present elliptic field calculations can now be compared to those from the local non-similarity solution and the experimental data [1]. These comparisons are shown in Fig. 4 for $y = 2.35$ cm and Fig. 5 for $y = 3.2$ cm. In general, the finite-difference calculations give better predictions of the temperature fields outside the flame sheet. Since both stations lie in the region where the effect of the preheated air layer can still be felt, part of the reason is that this effect is taken into account in the finite-difference calculations. There is, however, also an indication that this effect is not fully accommodated even in the finite-difference calculations. As seen in Fig. 5, the finite-difference results compare much better with the experimental data at this higher y-value of 3.2 cm where the preheated air layer effect is reduced almost to insignificance.

In the region inside the flame sheet at both levels of y, where the effect of preheated air layer is not expected to be important, neither the finite-difference calculations nor the local non-similarity solution has any particular advantage, when their results are compared to the experimental data. One exception is the prediction of the peak temperature, for which the local non-similarity solution is decidedly better. In this region, the finite-difference solution suffers from the fact that very fine values of Δx must be used for accuracy due to the large gradients there, while the local non-similarity solution as represented by the two-equation model also has obvious deficiencies, especially in situations where deviations from the similarity solution are large. Another difficulty encountered here is that the experimental data evidently indicate that there is a non-zero flame sheet thickness even for the methane diffusion flame, contrary to that in the mathematical formulation of the present problem. Therefore, a more refined analysis taking into account finite reaction rates in the combustion process is needed before the relative merits of the two solutions can be determined for calculations inside the flame sheet.

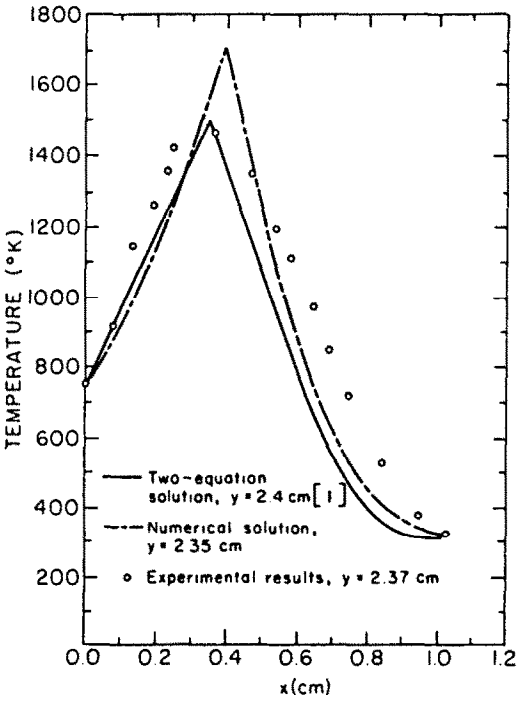

FIG. 4. Comparison of calculated temperature profiles with experimental data at $y = 2.37$ cm.

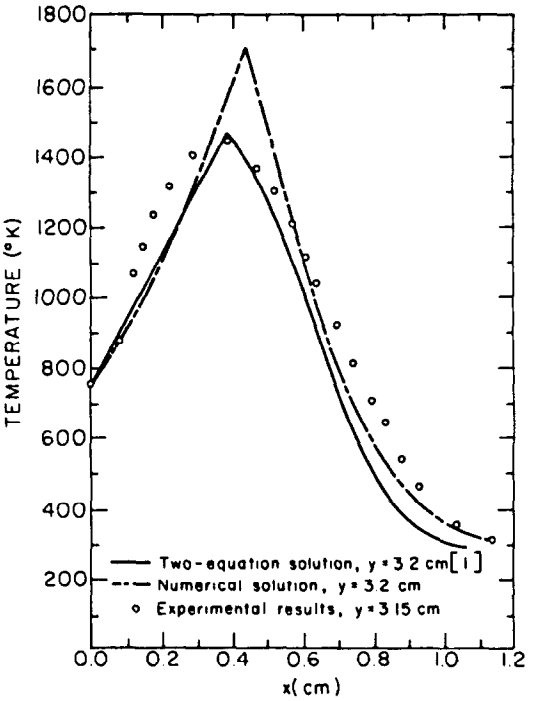

FIG. 5. Comparison of calculated temperature profiles with experimental data at $y = 3.15$ cm.

Finally, it is also noteworthy that the present study demonstrates the applicability of elliptic field or finite-difference calculations, which are normally utilized in recirculating or complex flow problems, even to boundary-layer problems. The chief advantage here is that deviations from any basic boundary-layer problem can be readily accommodated by such calculations. Good examples are high-order boundary-layer effects and problems involving boundary-layer types of singularities. It is in this sense that elliptic field or finite-difference calculations can be regarded as a unified tool for convection problems.

CONCLUSIONS

This numerical study deals with the phenomenon of a diffusion flame on a vertical plate burner with methane injection. The unsteady elliptic governing conservation equations along with an exponential wide-band model for gas radiation and an infinite reaction rate model for combustion are solved by an upwind finite-difference method utilizing staggered cells, pressure correction and a non-uniform cell structure in the computation domain. The results are compared with those of both the local non-similarity boundary-layer solution and the experimental data obtained in a previous study. The numerical results demonstrate that the thermal boundary-layer thicknesses are affected by the preheated air layer below the burning plate leading edge. However, the effect is essentially limited to the lower half of the porous plate. The finite-difference calculations also predict the temperature field outside the flame sheet better than the boundary-layer solution. This advantage vanishes in the region between the flame sheet and the wall. In this same region both methods of solution underestimate the temperature, and this is mainly due to the fact that the experimental data show a non-zero thickness for the flame sheet. Finally, the present study also demonstrates the applicability of the elliptic field calculation method to boundary-layer problems, thus broadening the scope of application of this method to all convection problems.

Acknowledgements—The authors gratefully acknowledge the support given by the National Science Foundation under Grant No. ENG76-81904 and CME79-18682 and by the Computing Center of the University of Notre Dame.

REFERENCES

1. K. V. Liu, J. R. Lloyd and K. T. Yang, An investigation of a laminar diffusion flame adjacent to a vertical flat plate burner, *Int. J. Heat Mass Transfer* **24**, 1959–1970 (1981).
2. A. M. Kanury, *Introduction to Combustion Phenomena*, p. 346. Gordon and Breach (1975).
3. J. O. Hirschfelder, C. F. Curtiss and R. B. Bird, *Molecular Theory of Gases and Liquids*, Chaps. 7 and 8. John Wiley, New York (1966).
4. R. B. Bird, W. E. Stewart and E. N. Lightfoot, *Transport Phenomena*, Chap. 16. John Wiley, New York (1960).
5. *Tables of Thermodynamic and Transport Properties*. Pergamon Press, New York (1960).
6. D. K. Edwards and W. A. Menard, Comparison of models for correlation of total band absorption, *Appl. Optics* **3**, 621–625 (1964).
7. C. L. Tien and J. E. Lowder, A correlation for the total band absorptance of radiating gases, *Int. J. Heat Mass Transfer* **9**, 698–701 (1960).
8. D. K. Edwards and S. J. Morizumi, Scaling of vibration-rotation band parameters for non-homogeneous gas radiation, *J. Quant. Spectros. Rad. Transfer* **10**, 175–178 (1970).
9. J. D. Felske and C. L. Tien, Infrared radiation from nonhomogeneous gas mixture having overlapping bands, *J. Quant. Spectros. Rad. Trans.* **14**, 35–48 (1974).
10. V. K. Liu, A numerical analytical and experimental investigation of the radiation-convection interaction in a diffusion flame adjacent to a vertical flat plate. Ph.D. dissertation, University of Notre Dame (1979).
11. S. V. Patankar, *Numerical Heat Transfer and Fluid Flow*, pp. 124–126 and 105–107. McGraw-Hill, New York (1980).

CALCUL DU CHAMP ELLIPTIQUE D'UNE FLAMME LAMINAIRE DE DIFFUSION ADJACENTE A UN BRULEUR PLAN ET VERTICAL

Résumé—Cette étude numérique porte sur le phénomène de diffusion de la flamme sur un brûleur plan vertical avec injection de méthane. Les équations de conservation instationnaire sont résolues par différences finies pour un modèle de rayonnement de gaz exponentiel à large bande et un modèle de vitesse de réaction infinie. Les résultats numériques sont comparés à ceux de la couche limite à non similarité locale, et aux données expérimentales d'une étude précédente. On montre que les calculs aux différences finies donnent des résultats en meilleur accord avec les données expérimentales dans la région externe de la couverture de flamme.

BERECHNUNG DES ELLIPTISCHEN FELDES EINER LAMINAREN DIFFUSIONSFLAMME AN EINEM SENKRECHTEN PLATTENBRENNER

Zusammenfassung—Diese numerische Untersuchung behandelt die Vorgänge in einer Diffusionsflamme an einem senkrechten Plattenbrenner mit Methaneinspritzung. Die instationären Erhaltungsgleichungen werden gemeinsam mit einem exponentiellen Breitbandmodell für die Gasstrahlung und einem infiniten Reaktionsmodell für die Verbrennung nach einem endlichen Differenzenverfahren gelöst. Die numerischen Ergebnisse werden dann sowohl mit den Werten der örtlich nicht-ähnlichen Grenzschichtlösung als auch mit experimentellen Ergebnissen verglichen, die aus vorhergehenden Untersuchungen gewonnen wurden. Es wird gezeigt, daß die Berechnungen nach dem endlichen Differenzenverfahren Werte ergeben, die im Gebiet außerhalb des Flammenbereiches besser mit den experimentellen Ergebnissen übereinstimmen.

РАСЧЕТ ЭЛЛИПТИЧЕСКОГО ПОЛЯ ЛАМИНАРНОГО ДИФФУЗИОННОГО ПЛАМЕНИ ГОРЕЛКИ, ВЫПОЛНЕННОЙ В ВИДЕ ВЕРТИКАЛЬНОЙ ПЛОСКОЙ ПЛАСТИНЫ

Аннотация — Проведено численное исследование ламинарного диффузионного пламени у вертикальной плоской горелки при подаче в нее метана. Нестационарные основные уравнения сохранения для экспоненциальной широкополосной модели излучения газа и бесконечной скорости реакции в случае горения решаются методом конечных разностей. Численные результаты затем сравниваются с результатами локального решения для неавтомодельного пограничного слоя и с экспериментальными данными ранее проведенного исследования. Показано, что расчеты методом конечных разностей позволяют получить результаты, которые лучше согласуются с экспериментальными данными в области, лежащей за пределами плоскости пламени.